remote sensing

MDPI

Article

Generalized Logistic Function: A Retracker to Improve the Accuracy of Water Level Time Series in Coastal Areas and Lakes

Arash Amini [1], Behzad Voosoghi [1], Mohammad Amin Khalili [2,*], Diego Di Martire [2], Shirzad Roohi [3] and Mahmoud Pirooznia [1]

[1] Faculty of Geodesy and Geomatics Engineering, K. N. Toosi University of Technology, Tehran 15433-19967, Iran; a_amini@email.kntu.ac.ir (A.A.); vosoghi@kntu.ac.ir (B.V.); ma.pirooznia@email.kntu.ac.ir (M.P.)
[2] Department of Earth Sciences, Environment, and Resources, University of Naples, Federico II, 80126 Naples, Italy; diego.dimartire@unina.it
[3] Innovation Solutions-GMV, 64295 Darmstadt, Germany; sroohi@gmv.com
* Correspondence: mohammadamin.khalili@unina.it; Tel.: +39-34-4413-7462

Abstract: The efficiency of satellite altimetry in monitoring coastal areas and lakes is limited due to the contaminated waveform caused by non-water features included in the satellite footprint. Therefore, to mitigate these limitations, waveforms need to be retracked. In this research, the Generalized Logistic Function (GLF) has been introduced with Analytical (GLFA) and Numerical (GLFN) approaches to retrack the first sub-waveform. The results have been compared with those obtained from on-board retrackers existing in Level-2 altimetry data, the retracking of the full-waveform, the first sub-waveform, and the mean of the sub-waveforms using the threshold retracker. The Level-2 and Level-1B data of the Sentinel-3A (SRAL) mission for passes 141, 700, 244, and 311, respectively, passing over Vättern and Hjälmaren Lakes in Sweden, and 0–2 km distance from the coasts of the Bay of Alcudia and the Northeast Gulf of Bothnia from January 2019 to December 2022, were investigated. The results of the retracking approaches used in this study were evaluated against tide gauge data in terms of RMSE and its improvement percentage. The results demonstrate the superiority of the GLFA over the GLFN in coastal areas, while over lakes, the results are nearly equivalent. The improvement percentages of RMSE for the GLFA and GLFN compared to on-board retrackers, respectively, are as follows: for Vättern Lake, 53% and 58%; for Hjälmaren Lake, 40% and 33%; for the Bay of Alcudia, 81% and 46%; and for the Northeast Gulf of Bothnia, the GLFA shows a 36% improvement, while the GLFN yields results equivalent to on-board retrackers. The GLF has shown better performance compared to other approaches, except for Vättern Lake, which yields results almost equivalent to the first sub-waveform retracking approach. Additionally, the mean of the sub-waveform retracking approach by making use of the threshold algorithm has mostly demonstrated weaker performance compared to other methods.

Keywords: retracking; logistic function; sub-waveform; satellite altimetry; sentinel-3A

Academic Editors: Milena Menna and Daniele Ciani

Received: 3 January 2025
Revised: 25 January 2025
Accepted: 31 January 2025
Published: 5 February 2025

Citation: Amini, A.; Voosoghi, B.; Khalili, M.A.; Di Martire, D.; Roohi, S.; Pirooznia, M. Generalized Logistic Function: A Retracker to Improve the Accuracy of Water Level Time Series in Coastal Areas and Lakes. *Remote Sens.* **2025**, *17*, 533. https://doi.org/10.3390/rs17030533

1. Introduction

Oceans cover 71% of the Earth's surface. Coastal areas are recognized as one of the most developed economic regions. Forty percent of the world's population resides within 100 km of the coast, with over 600 million people living at elevations of 10 m or less above sea level. It is expected that the population in these areas will increase by 25% by the year 2050 [1,2]. Freshwater contributes up to 3% of the Earth's water, with only 0.3% of that being surface water. From this surface water, 87% is allocated to lakes [3]. Lakes

serve not only as a vital source of drinking water but also play a crucial role in agriculture, supporting the ecosystems of animals and birds and preserving natural processes and ecosystems. However, lakes can pose risks, including natural disasters such as floods [4,5]. Therefore, monitoring changes in lakes water and coastal areas is essential and represents an important area of research.

Changes in water level relative to a local datum are traditionally measured using a device called a 'tide gauge'. Tide gauges are installed in coastal environments or protected islands; hence, they are unable to monitor water level changes in remote offshore areas [4]. This tool also faces other limitations, such as vulnerability to natural disasters like floods, limited data access due to political restrictions, and the inability to monitor water levels in remote and mountainous areas. Additionally, the high expense of procurement and maintenance has led to a reduction in hydrological monitoring networks in recent years. This has raised concerns among scientific communities due to the necessity of water resource management. Satellite altimetry addresses all these limitations by providing continuous, stable, repeatable, and highly accurate measurements of water levels in any weather condition, day or night [5–7].

The radar altimeter emits electromagnetic pulses towards the surface and measures the reflected power from that surface. The collected power measurements over time of interactions with the surface are called a 'waveform'. Waveforms are the primary measurements in satellite altimetry. Satellite altimetry is a technique primarily developed for monitoring water levels in oceanic regions. Brown (1977) introduced a model for the pulse return signal from the ocean surface [8]. Therefore, oceanic waveforms serve as a criterion measure of signal travel time and, consequently, the satellite's distance from the water surface. By measuring this distance and knowing the satellite's altitude, the surface height relative to a reference datum can be determined [4,8].

In coastal areas and lakes monitoring, due to the large satellite footprint, shallow depth, and the presence of non-water features in the satellite footprint (such as large rocks and vegetation cover), the recorded waveforms become contaminated and deviate from oceanic waveforms. Consequently, in these areas, the distance between the satellite and the water surface, and thus the reported surface height, is inaccurate. To address this issue, retracking algorithms are employed to retrieve the correct signal travel time in these areas [3,9].

In this field, early studies have introduced the β-parameter retracking algorithm (five and nine parameters) to retrack the reflected waveforms from the ice sheets in the South Pole and Greenland using Seasat-1 satellite altimetry data [10]. The Offset Center of Gravity (OCOG) is a statistical retracking algorithm sensitive to surface topography features, utilizing the center of gravity and a rectangular waveform assumption [11]. The threshold retracking algorithm has been proposed to study changes in the elevation of ice sheets [12].

Later, studies on various reflections from the surface in the waveform under the title 'meaningful sub-waveform' were pursued. In the study of Taiwan's coasts, using the Geosat altimetry mission, two improved threshold retracking methods have been introduced. The water level of meaningful sub-waveforms has been calculated by applying the threshold retracker. In one of these methods, a water level closer to the previous waveform's water level was selected [13], while in the other method, a meaningful sub-waveform with a water level closer to a reference height was chosen [14]. Both methods demonstrate superiority over the full-waveform retracking method using the threshold and 5β parameter retrackers. In another study using the T/P mission data on Lake Hulun, an improved threshold retracker, 5β-parameter, and Nβ-parameter were applied to meaningful sub-waveforms. The results indicate a better performance for the improved threshold retracker

over the full-waveform retracking method using the threshold, OCOG, 5β-parameter, and 9β-parameter methods [15]. Retracking the meaningful sub-waveform with the highest correlation to the reference sub-waveform by using the threshold retracker is proposed. Implementing this method to monitor the Antarctic Ocean using ERS-1 satellite data has shown better results compared to full-waveform retracking using the threshold and 5β-parameter algorithms [16]. With the reasoning that the first meaningful sub-waveform can be the one without ambiguity that reflects from the nadir, some studies follow retracking via this sub-waveform:

The retracking of the first meaningful sub-waveform using the threshold and OCOG retrackers has yielded better results compared to the full-waveform retracking method using the threshold, OCOG, 5β-parameter, and Level-2 on-board retracker in the CryoSat-2 (SAR) mission for studying the arctic region [17]. The water level of the Ukai reservoir was investigated using SARAL satellite data. This research found that the first meaningful sub-waveform with a threshold of 50% has optimal results compared to other retrackers: the 5β-parameter, ICE-2, OCOG, and threshold were 50% [18]. In [19], the MWaPP (Multiple Waveform Persistent Peak retracker) algorithm was introduced. In this algorithm, the first meaningful sub-waveform in the average waveform serves as the optimal criterion for identifying optimized sub-waveforms among other waveforms. Studies [9,20] have also pursued the retracking of the first sub-waveform using the threshold algorithm, comparing it with the full-waveform retracking method using other retracker methods.

On the other hand, studies have shown that the first sub-waveform is not always optimal. In the study of various aquatic regions, using different altimetry missions and retracking algorithms including mathematical, physical, empirical, and statistical methods, the threshold retracker has been proposed [21,22]. Additionally, for monitoring the water level of small aquatic regions with complex shapes, the mean sub-waveform retracking approach followed by the first sub-waveform retracking approach has been recommended [21,22]. In studying Lake Vänern using the Sentinel-3A altimetry mission, sub-waveforms were retracked using the threshold retracker, and an optimal sub-waveform with a water level feature closer to the in situ gauge was selected. The results of this method show a 50% improvement in the accuracy of water level time series compared to on-board retrackers and are almost equivalent to the mean sub-waveform retracking approach. Optimal sub-waveform analysis shows that in more than 90% of the waveforms, the first sub-waveform is identified as optimal [3]. The symmetry point of the spline function is introduced as the correct moment for signal return from the surface in the study of coasts of Sweden and the Sea of Oman using the Jason-1 and Jason-2 missions [23]. The OCOG and threshold methods for the full-waveform, as well as the first sub-waveform with the threshold algorithm and the ALES (the Adaptive Leading Edge Sub-waveform) retracker [24], were also evaluated. Results show that the proposed method had a significant improvement compared to other methods [23].

The logistic function was introduced by Pierre-François Verhulst (1804–1849), and his work on population growth in the 19th century is well known [25–28]. The logistic function is implemented in various fields, such as predicting economic and trade market trends [29], enhancing image filters [30], modeling power curves for wind turbines [31], exact solutions of nonlinear differential equations [32], and estimating the trend of the COVID-19 pandemic spread [33]. The generalized logistic function (GLF) is derived by solving the first-order ordinary Riccati differential equation with constant coefficients. Its initial and final parts are constant, while the middle part is ascending. The initial and final parts define the minimum and maximum values of the function, respectively. The middle part, with the slope and position of the midpoint, is also specified. The GLF converges to

the logistic function when the minimum value is zero. Both the logistic and its generalized form are kinds of sigmoid or S-shaped curves [34].

In this study, the GLF, due to its simplicity and agreement in parameters and geometry with satellite altimetry waveforms, is used as a retracker with two approaches: Numerical (GLFN) and Analytical (GLFA). The water levels derived from on-board retrackers, full-waveform, first sub-waveform, and mean sub-waveform retracking methods using the threshold retracker, GLFA, and GLFN were compared. It is worth noting that, even though the ALES is recognized as a powerful retracker in generating water level time series in coastal areas, in our previous studies [9]. we compared the first sub-waveform (original waveform) retracking approach using the threshold retracker to ALES, and we found that our method has a better performance than ALES. In this study, we compared the GLF with the first sub-waveform (original waveform). So, indirectly the comparison has been performed with ALES. On the other hand, ALES cannot provide us with reliable data in 0–2 km distance from the coast. So, we removed it from the further process in this study. The Sentinel-3A mission data on Vättern Lakes and Hjälmaren in Sweden, Bay of Alcudia in northeastern Mallorca Island, and the Northeast Gulf of Bothnia within 0–2 km of the coast were used for this evaluation. The results demonstrate a better performance of the proposed method compared to other investigated methods, including on-board retrackers existing in Level-2 of the Sentinel-3A altimetry mission, full-waveform, first, and mean sub-waveform retracking using the threshold retracker.

2. Materials and Methods

2.1. Datasets

2.1.1. Sentinel-3A (SRAL)

Copernicus is a European program for monitoring the Earth. The space segment of this project includes different Sentinel satellites. Sentinel-3A, as the third mission, was launched by the European Space Agency (ESA) in February 2016. The main objective of this mission is to measure sea and land surface temperatures using the Sea and Land Surface Temperature Radiometer (SLSTR) instrument. In addition, it measures ocean and land surface color with the Ocean and Land Color Instrument (OLCI) and monitors sea surface topography by taking advantage of a Synthetic aperture Radar ALtimeter (SRAL). The SRAL instruments include a combination of a MicroWave Radiometer (MWR) and a Precise Orbit Determination (POD) toolset. The SRAL altimeter is a dual-frequency instrument (Ku and C bands) operating in a Synthetic Aperture Radar (SAR) mode; it measures the round-trip time of the radar pulse transmitted and reflected from the surface with an accuracy better than a nanosecond [35]. This altimeter was first introduced as the Delay-Doppler altimeter in 1998 [36]. Such an altimeter with its high Pulse Repetition Frequency (PRF), as well as its along-track and multi-look processing capabilities, achieves high spatial resolution along the track (up to 250 m) and reduces speckle noise. It also increases the precision of range measurements. The reduction in the footprint along the track results in less contamination of waveforms by land, which is advantageous for monitoring coastal areas and inland water bodies [37–39]. In this study, Level-1B (SR-1-SRA) and Level-2 (SR-2-LAN) data of the Sentinel-3A mission with Non-Time Critical (NTC) temporal access for the period from January 2019 to December 2022, corresponding to cycles 40 to 93, were used. These data are accessible from https://browser.dataspace.copernicus.eu/ (accessed on 15 November 2023). Table 1 introduces some characteristics of this mission.

Table 1. Characteristics of the Sentinel-3A mission [35,40].

Altimeter	Launch	Mode	Altitude (km)	Inclination(deg)	Revisit Time (day)
SRAL	February 2016	SAR	814.5	98.65	27
PRF (KHz)	**Pulse Length (ns)**	**Cycle Length (orbits)**		**Bands (GHz)**	**Ground Track Separation at Equator (km)**
17.8	3.125	385		Ku (13.6), C (5.4)	104

2.1.2. Tide Gauge Datasets

To evaluate the accuracy of the time series of water levels derived from the satellite altimetry mission, data from tide gauges installed in the study area were used. Table 2 shows the specifications of the tide gauges used in this research. The tide gauge data for lakes are available at https://www.smhi.se/q/Stockholm/2673730 (accessed on 11 December 2023), and for coastal areas, they are available at https://marineinsitu.eu/dashboard/ (accessed on 7 January 2024).

Table 2. Specifications of the tide gauges used in this research.

Area	Station	Datum	Sampling Rate	Lat, Lon(deg)	Approximate Distance from the Satellite Pass (km)
Vättern Lake	Motala	RH00	Daily	58.5345,15.0419	7
Hjälmaren Lake	Hjälmaren	RH00	Daily	59.2727,16.2968	30
Bay of Alcudia	IR_TS_TG_AlcudiaTG	Harbor	60 min	39.8347,3.1391	9
Northeast Gulf of Bothnia	BO_TS_TG_Raahe	MSL	60 min	64.6659,24.4071	15

2.2. Case Studies

2.2.1. Vättern Lake

Vättern Lake is the second-largest lake in Sweden and the fifth-largest lake in Europe [41]. Due to its boat-like shape and sensitivity to changes in wind and atmospheric pressure, it has strong currents with wave amplitudes reaching 20 to 25 cm. With an area of 1856 km^2, an average depth of 39.9 m, a shoreline length of 642 km, and being located in the central southern part of Sweden, it is considered a significant asset and a suitable water source for industrial activities [42].

2.2.2. Hjälmaren Lake

Hjälmaren Lake, with an area of 478 km^2, has an average depth of 6.1 m and a shoreline length of 428 km. It is located in Sweden in an area with ancient rock formations. The surrounding deposits of the lake, dominated by lime-rich clay soil, have made the adjacent areas suitable for cultivation. Additionally, agriculture around the lake contributes to nutrient supply to the water. This lake, with shallow depths, consists of four main basins separated by islands and serves as a source of freshwater and recreational activities [42].

2.2.3. Bay of Alcudia

The Spanish Island of Mallorca, in the western Mediterranean, belongs to the Balearic Island's archipelago. With an area of 3603 km^2 and a coastline length of 550 km, this island is situated about 170 km from the Spanish mainland. One hundred eighty bays are spread relatively evenly along its coastline. Excluding the offshore islands of Cabrera Island on the south coast of Mallorca and the island of Sa Dragonera on the southwest coast of Mallorca, Mallorca is the largest island among the islands in Balearic [43]. In this study, the Bay of Alcudia, located in the northeastern part of this island, was investigated.

2.2.4. Northeast Gulf of Bothnia

The Gulf of Bothnia, as the northern arm of the Baltic Sea, covers an area of approximately 117,000 km^2. This gulf is bordered by Finland to the east and Sweden to the west. Despite extending 725 km from north to south, its east–west span varies from 80 to 240 km. The gulf reaches its maximum depth of 295 m in the west-central part and has an average depth of about 60 m. Due to the inflow of numerous rivers such as Ångerman, Ume, Lule, Torne, Kemi, and Oulu, it has very low salinity and consequently experiences ice cover for up to 5 months in winter [44]. In this research, the northeastern part of the Gulf of Bothnia was studied.

In this study, data from 141, 700, 244, and 311 passes of the Sentinel-3A mission were processed, corresponding to passes over Vättern Lake, Hjälmaren Lake, the Bay of Alcudia, and the Northeast Gulf of Bothnia, respectively. Figure 1 illustrates the satellite passes and the locations of tide gauges in the study areas.

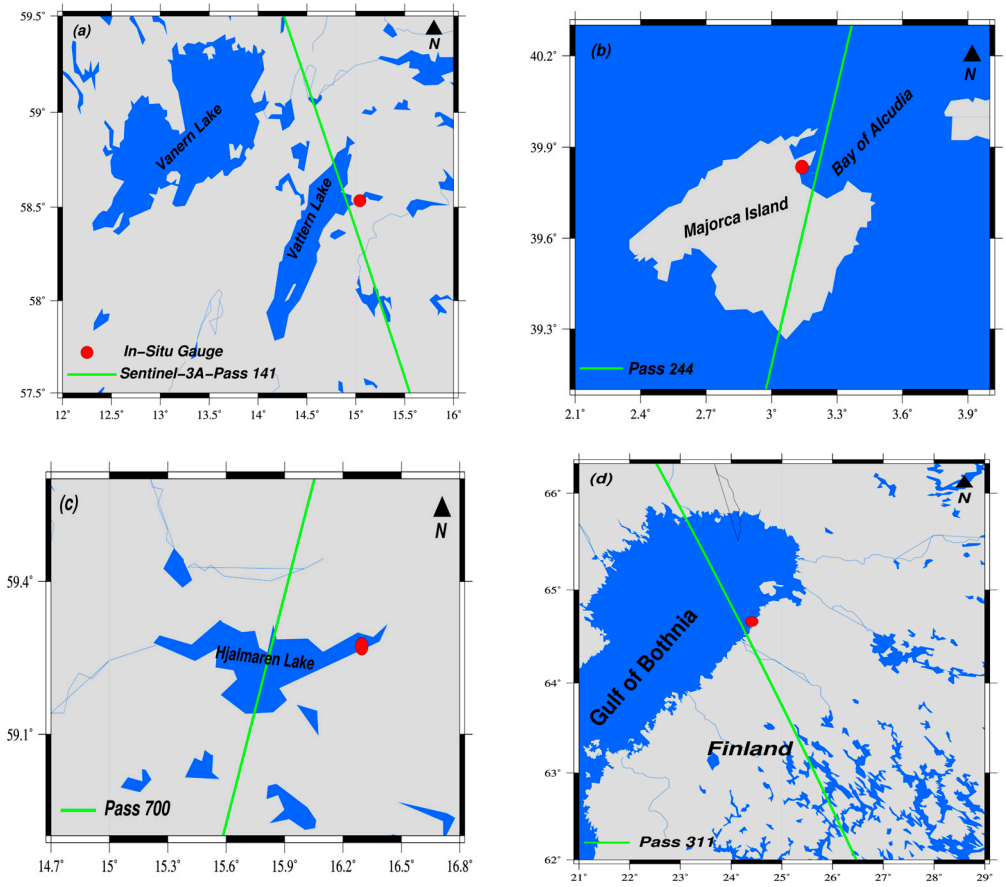

Figure 1. Sentinel-3A passes' orientation and the locations of tide gauges in the study areas; (**a**) Vättern Lake, (**b**) the Bay of Alcudia, (**c**) Hjälmaren Lake, and (**d**) the Northeast Gulf of Bothnia.

2.3. Principles of Satellite Radar Altimetry

Altimeter satellites emit electromagnetic pulses with a specific power and frequency towards the surface. After these pulses hit the surface, a part of them is back reflected to the altimeter. By measuring the travel time (t) of the pulse and multiplying half of it by the speed of light (C), the distance from the satellite's center of mass to the surface (R) is calculated (Equation (1)) [21]. The power of the reflected pulse to the altimeter based on the interaction time of the pulse with the surface is called the waveform [7]. The interaction time of the pulse with the surface is divided based on the pulse length (τ) and is called the gate [7]. The moment of the pulse's return from the surface is considered based on the oceanic waveform (also known as the Brown model) and is called the nominal gate [3].

In other words, the nominal gate is the middle of the leading edge for an ideal oceanic waveform. If the surface deviates from oceanic conditions such as shallow depth and non-water features in the satellite footprint, the nominal gate (G_{nom}) reports the moment of return from the surface incorrectly [3,9,45]. Therefore, the correct moment of the reflected pulse from the surface (retracked gate) must be retrieved (G_{ret}). This correction, introduced in Equation (2), is called the retracking correction [9]. Due to the interaction of the pulse with the atmosphere and the presence of gravitational forces, ionospheric (C_{iono}), wet tropospheric ($C_{wet-tropo}$), dry tropospheric ($C_{dry-tropo}$), solid earth tide ($C_{solid-earth-tide}$), pole tide ($C_{pole-tide}$), load tide ($C_{load-tide}$), sea state bias ($C_{sea-state-bias}$), and geoid (C_{geoid}) corrections are applied to this measured range [6,9]. From the altitude of the satellite to a specific reference surface such as WGS84 (H) and corrected measured range, the instantaneous Water Level (WL) can be obtained from Equation (3) [3,9].

$$R = C\frac{t}{2} \tag{1}$$

$$C_{ret} = (G_{ret} - G_{nom})C\frac{\tau}{2} \tag{2}$$

$$\begin{aligned} WL = H - R - (&C_{ret} + C_{iono} + C_{dry-tropo} + C_{wet-tropo} + C_{solid-earth-tide} \\ &+C_{pole-tide} + C_{load-tide} + C_{sea-state-bias} + C_{geoid}) \end{aligned} \tag{3}$$

It should be noted that for the lakes assessed in this research, geoid, pole tide, and solid earth tide corrections are considered. For the coastal areas, in addition to these, load tide and sea state bias corrections are also applied [3,46]. In both cases, atmospheric corrections were implemented.

2.4. Retracking Approaches

In monitoring lakes and coastal areas where the altimeter footprint includes non-water features, the return waveform could have more than one leading edge (sub-waveform or peak) [9,22], but not all of these sub-waveforms are meaningful. In this research, the meaningful sub-waveforms were identified and surveyed based on the procedure outlined in [18]. Figure 2 illustrates the meaningful sub-waveforms identified in some of the waveforms from the study areas. In this research, for simplicity, the meaningful sub-waveform is called the sub-waveform or peak. Previous studies have proposed various approaches to retrack these waveforms. In this study, retracking approaches were employed, including full-waveform (using on-board and threshold retrackers), first sub-waveform (utilizing threshold and GLF retrackers), and mean sub-waveform (applying the threshold retracker).

2.4.1. Full-Waveform Retracking

In the full-waveform retracking approach, all parts of the waveform are involved to find the correct moment that the signal returns from the surface, termed the retracked gate. The Level-2 data of the Sentinel-3A (SRAL) mission offers ranges from the OCOG/Ice-1, Ice-sheet, Sea-ice, and Ocean retrackers, called on-board retrackers. These algorithms retrack the full-waveform. The OCOG/Ice-1 retracker computes the waveform amplitude using the OCOG retracking algorithm and considers the gate corresponding to 80% of this amplitude as the retracked gate [46]. The Ice-sheet retracker is designed specifically for retracking waveforms over ice sheets and operates by fitting a modified Gaussian semi-analytical model to the waveform using the least squares method. Various parts of the waveform are modeled using five piecewise continuous functions in this retracker [46,47]. The Sea-ice retracker is designed for retracking waveforms in sea–ice regions. In this retracker, the leading edge part of the waveform is modeled with a Gaussian function, the trailing edge part with a declining exponential function, and the middle part with a function

that connects the leading and trailing edge parts [46,47]. The Ocean physical retracker is designed for studying coastal and oceanic regions. This retracker computes the retracking gate by numerically fitting the SAR waveform model (SAMOSA) to the waveforms [46,47]. In full-waveform retracking using the threshold retracker, the amplitude parameter is derived from the whole waveform using the OCOG retracking method, and a percentage of this amplitude (the threshold) will be the retracked gate [12,21,22].

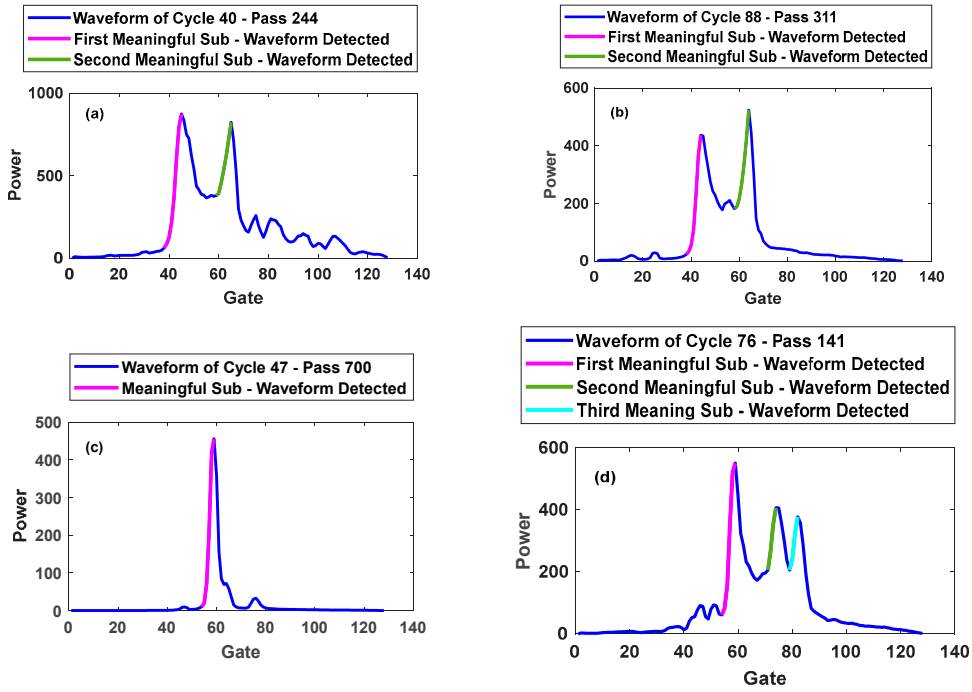

Figure 2. Meaningful sub-waveform identification in the waveforms; (**a**) Cycle 40 of pass 244 in the Bay of Alcudia; (**b**) Cycle 88 of pass 311 in the Northeast Gulf of Bothnia; (**c**) Cycle 47 of pass 700 in Hjälmaren Lake; (**d**) Cycle 76 of pass 141 in Vättern Lake.

2.4.2. First and Mean Sub-Waveform Retracking

In waveforms with more than one leading edge, the computed amplitude is not necessarily related to the maximum power of the waveform, and the retracked gate may not be accurately determined. In the first sub-waveform retracking approach, it is assumed that only one sub-waveform is related to the reflection from the water surface, and the first sub-waveform is merely a clear reflection at the nadir location [18,22]. However, in the mean sub-waveform retracking approach, it is assumed that not only one sub-waveform is related to the reflection from water, but different sub-waveforms from various parts of the water surface within the radar footprint are reflected [6,21,22]. Therefore, their mean retracked correction is considered. In sub-waveform (first and mean) retracking using the threshold retracker, the amplitude parameter is the maximum power of the sub-waveform/sub-waveforms, and a percentage of this amplitude will be the retracked gate.

2.5. Generalized Logistic Function

The Generalized Logistic Function (GLF) is a solved first-order ordinary differential equation, known as the Riccati equation, with constant coefficients [34]. This function has an initial segment with the minimum value, a terminal segment with the maximum value, and an ascending middle segment (Figure 3a). This function is called logistic when the minimum value is zero (Figure 3b) [34]. Equation (4) represents the mathematical form of this function [34].

$$u(t) = u_{\min} + \frac{u_{\max} - u_{\min}}{1 + \exp(-s(t-g))} \quad (4)$$

In Equation (4), t is the time, $u(t)$ is the value of the function, and $u_{\min}$ and $u_{\max}$ represent the minimum and maximum values of the function, respectively. Variable s is the slope of the ascending segment, and g represents the inflection point of this function.

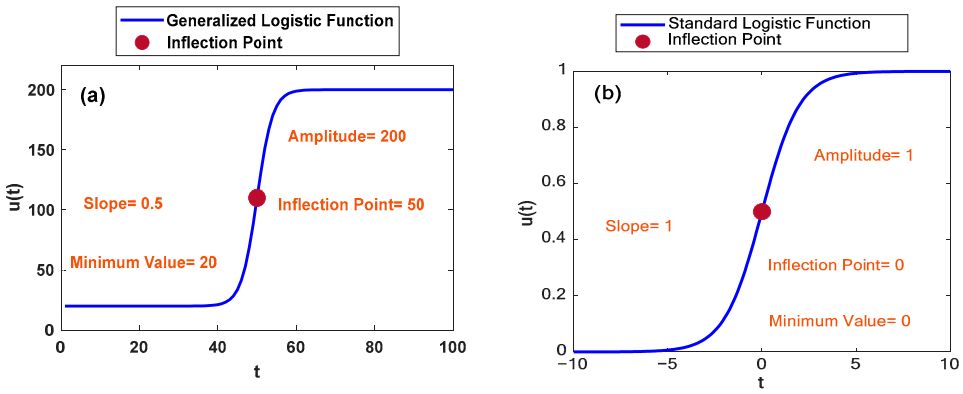

Figure 3. The generalized logistic function and logistic function; (**a**) the generalized logistic function for $u_{\min} = 20$, $u_{\max} = 200$, $s = 0.5$, and $g = 50$; (**b**) the logistic function for $u_{\min} = 0$, $u_{\max} = 1$, $s = 1$, and $g = 0$.

Figure 3a demonstrates the similarity of the GLF with the waveforms of satellite altimetry in the initial and ascending parts. Moreover, the mathematical form of this function suggests the possibility of a parameter equivalent to the parameters of the waveform. Thus, $u_{\min}$ can be equivalent to thermal noise as the initial part of the waveform (p_n), s to the leading edge slope, $u_{\max}$ to the amplitude (a), and g to the retracking gate in the waveform. Therefore, this function can be used as a retracker to determine the parameter g as the retracked gate. Furthermore, this function is characterized by a simple mathematical equation, which increases its efficiency. In this study, we calculate the retracking gate from the GLF through both numerical and analytical approaches.

2.5.1. Elimination of Ambiguous Waveforms

The GLFA and GLFN approaches are based on fitting a mathematical function to the waveform. Therefore, for suitable fitting, the waveforms were smoothed using a moving average filter with a size of three [46–48]. Based on studies [3,6,21–23], the first sub-waveform is not always the optimal selection for retracking. In order to investigate this issue, statistical information on the number of multi-peak waveforms is provided. Furthermore, according to the procedure followed in [3], statistical information about the optimal sub-waveform (the sub-waveform with water levels closer to the tide gauge data) in the study areas is also provided. In this research, where the selection of the first sub-waveform is ambiguous, the waveforms were not processed. To determine this ambiguity, the GLF fitted to the first sub-waveform and the other waveforms were normalized. Then, the dissimilarity parameter between the GLF and the waveform in the first sub-waveform was computed [46–48]. Waveforms with dissimilarity parameters greater than 60 were excluded from processing [46,48]. The threshold value of 60 has been empirically determined and is also used in [46,48]. Equation (5) introduces the dissimilarity parameter [48].

$$diss = \frac{\sum_{i=1}^{N} (W_i - Y_i)^2}{r(W_{1,2,\ldots,N}, Y_{1,2,\ldots,N})} \quad (5)$$

In Equation (5), W_i is the waveform, Y_i is the fitted GLF, N is the number of first sub-waveform gates, and $r(W_{1,2,\ldots,N}, Y_{1,2,\ldots,N})$ is the correlation between the waveform and the GLF in the first sub-waveform. Table 3 and Figure 4 show the percentage (%)

of unambiguous waveforms after applying the dissimilarity criterion and the computed dissimilarity parameter for the waveforms, respectively.

Table 3. The percentage (%) of unambiguous waveforms after applying the dissimilarity criterion.

Approach/Case Study (Pass)	Bay of Alcudia (244)	Northeast Gulf of Bothnia (311)	Hjälmaren Lake (700)	Vättern Lake (141)
GLFA	80.70	93.97	91.13	87.09
GLFN	75.32	91.43	88.99	86.90

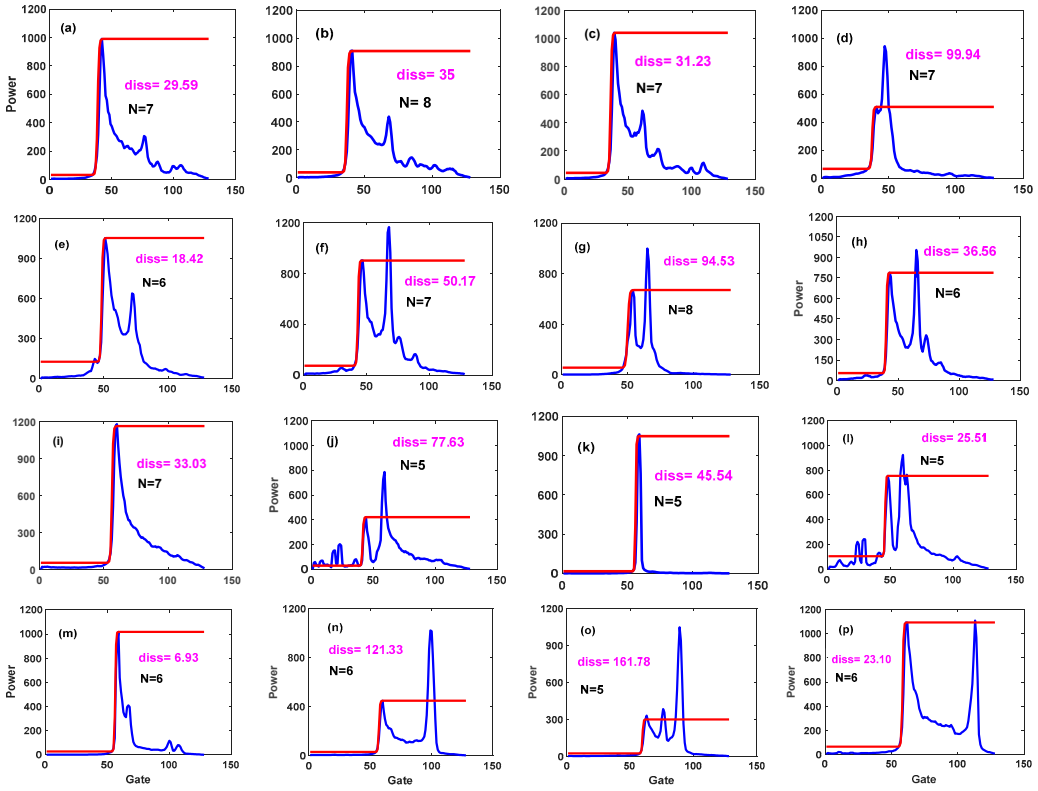

Figure 4. The dissimilarity parameter computed between the waveform (blue) and the GLF (red) in the first sub-waveform; (**a**–**d**) the examples for pass 244 for the Bay of Alcudia; (**e**–**h**) pass 311 for the Northeast Gulf of Bothnia; (**i**–**l**) pass 700 for Hjälmaren Lake; (**m**–**p**) pass 141 for Vättern Lake.

Table 3 shows that the dissimilarity criterion with a threshold of 60 identifies more than 75% of the waveforms with the first unambiguous sub-waveform (unambiguous waveforms) in all study areas.

2.5.2. Analytical Approach

In the GLF with an Analytical (GLFA) approach, the function is fitted to the first sub-waveform using the least squares method in which the slope of the leading edge and the retracked gate are estimated. The primary gate and the maximum power of the first sub-waveforms are considered as the minimum $u_{\min}$ and maximum $u_{\max}$ values of the function, respectively. Equation (4) is a nonlinear least squares problem that requires an initial value to estimate unknown parameters. By substitution the variable, the issue is transformed into a linear equation which can be solved. First, Equation (4) is rewritten as Equation (6). Then, the logarithm in base neper (e) is applied on both sides of Equation (6),

leading to Equation (7). By substituting the variables according to Equation (8), the equation is transformed into a linear form (Equation (9)).

$$\frac{a - p_n}{u(\mathrm{t}) - p_n} - 1 = \exp\left(-s\,(\mathrm{t} - g)\right) \tag{6}$$

$$Ln\left(\frac{a - p_n}{u(\mathrm{t}) - p_n} - 1\right) = -s\mathrm{t} + sg \tag{7}$$

$$L = Ln\left(\frac{a - p_n}{u(\mathrm{t}) - p_n} - 1\right) \quad E = sg \quad D = -s \quad X = t \tag{8}$$

$$L = DX + E \tag{9}$$

Implementing the linear least squares principle with a design matrix A and observation vector L, the unknowns (D, E) can estimated from Equation (10) [49]. Finally, the unknowns (s, g) can be estimated from Equation (11). Figure 5 shows the fitted GLFA to the first sub-waveform for some of the waveforms from the study areas.

$$X = \left(A'A\right)^{-1}A'L \tag{10}$$

$$s = -D \quad g = -\frac{E}{D} \tag{11}$$

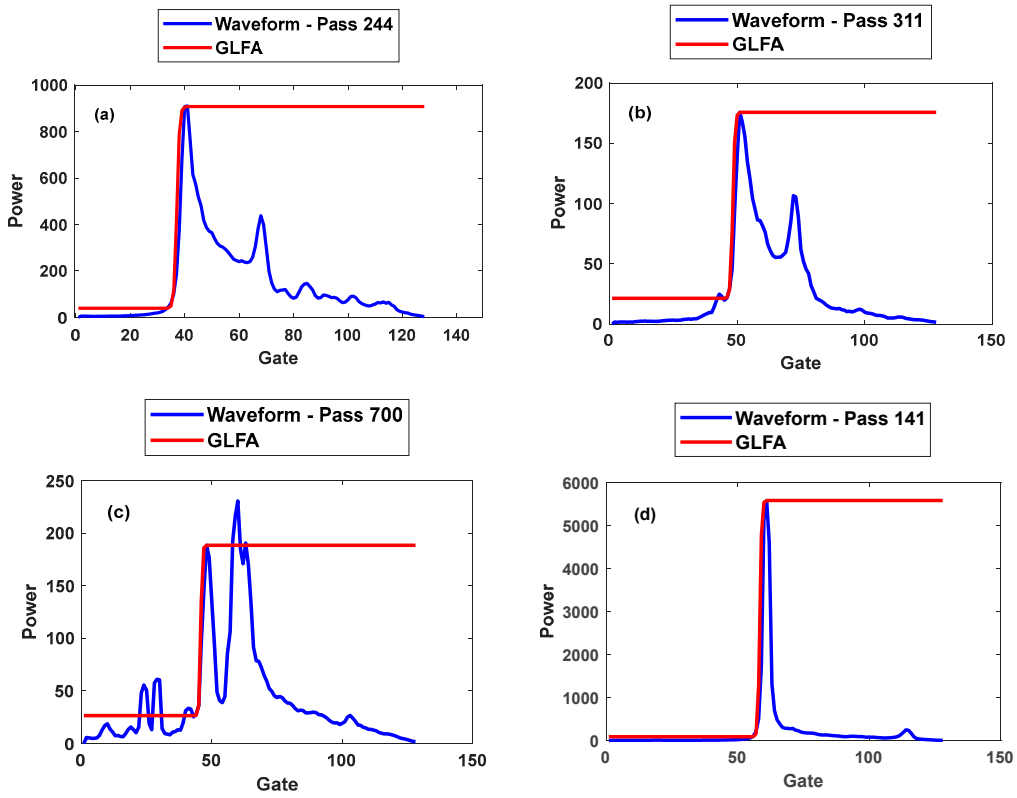

Figure 5. Fitted GLFA to the first sub-waveform in the study areas; (**a**) pass 244 for the Bay of Alcudia; (**b**) pass 311 for the Northeast Gulf of Bothnia; (**c**) pass 700 for Hjälmaren Lake; (**d**) pass 141 for Vättern Lake.

2.5.3. Numerical Approach

In the GLF with Numerical approach (GLFN), the minimum and maximum values of the function are selected according to the GLFA approach. The sum of the power differences between the neighboring gates in the first sub-waveform is considered as s. The first sub-waveform is interpolated with intervals of 0.02 gates (equivalent to an accuracy of 1 cm),

and the GLF is formed for each interpolated gate g. The retracked gate is the gate for which the GLF has the maximum Correlation coefficient (Corr) with the first sub-waveform. In addition to the maximum correlation parameter, the minimum of the Mean Absolute Error (MAE) and the Root Mean Square Error (RMSE) is also evaluated when comparing the GLF and the first sub-waveform. The mathematical formulations of this approach are described in Equation (12).

$$\begin{aligned} &u_1^1(\mathrm{t}) = p_n + \tfrac{a-p_n}{1+\exp\,(-s\,(\mathrm{t}-g_1))},\, u_2^1(\mathrm{t}) = p_n + \tfrac{a-p_n}{1+\exp\,(-s\,(\mathrm{t}-g_2))} \cdots \\ &u_q^m(\mathrm{t}) = p_n + \tfrac{a-p_n}{1+\exp\,(-s\,(\mathrm{t}-g_q))},\; q = 1,\ldots,i,\; m = 1,\ldots,j \\ &\text{Optimum}\,(\mathrm{g}^m) = \left\{ g_q^m \middle| \text{maxcorr}\left(u_q^m(\mathrm{t}),\ \text{first sub waveform}\,(m)\right)\right\} \end{aligned} \tag{12}$$

In Equation (12), i is the number of interpolated gates in the first sub-waveform and j is the number of waveforms. Figure 6 shows the fitted GLFN to the first sub-waveform for some of the waveforms from the study areas. The estimates of the GLFA (retracking gate and ascending slope) are influenced by the incomplete fitting of the function to the ascending part of the waveform, whereas in the GLFN, the ascending slope is computed from the waveform, and the retracking gate is obtained through a step-by-step evaluation of the ascending part. The performance of the GLFN approach depends on determining the slope of the ascending section, selecting the step size for the retracking gate assessment, and defining the evaluation parameter to identify the optimal retracking gate. In contrast, the GLFA approach estimates the retracking gate and the slope of the leading edge simultaneously.

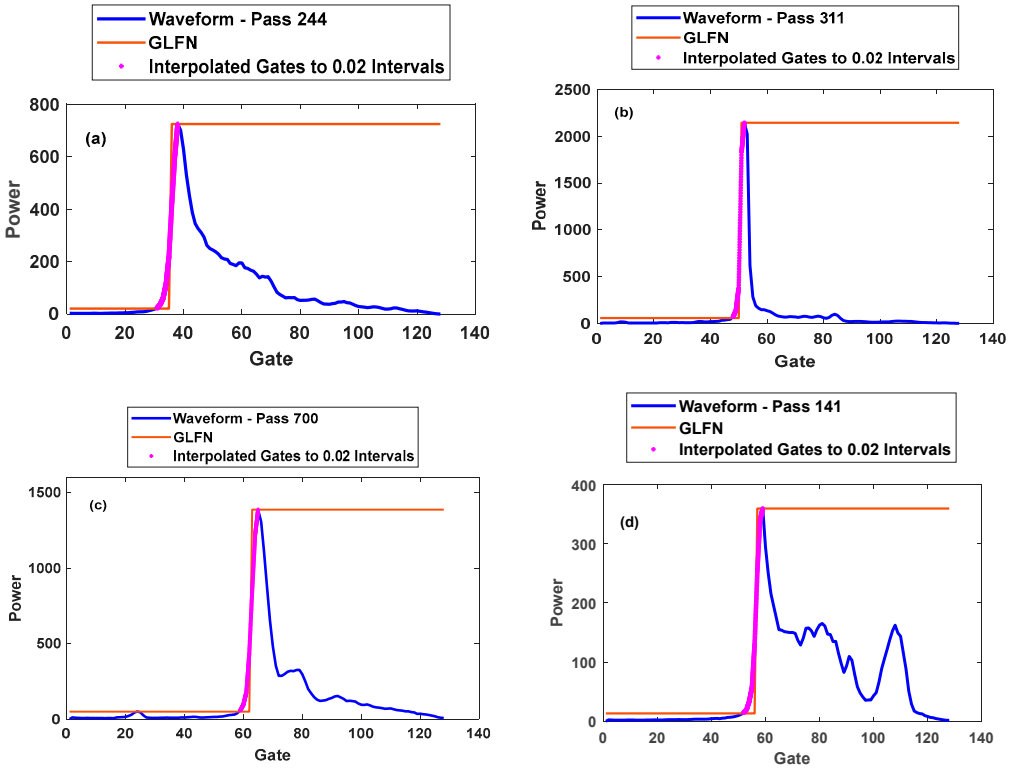

Figure 6. Fitted GLFN to the first sub-waveform in the study areas; (**a**) pass 244 for the Bay of Alcudia; (**b**) pass 311 for the Northeast Gulf of Bothnia; (**c**) pass 700 for Hjälmaren Lake; (**d**) pass 141 for Vättern Lake.

Figure 7 illustrates the retracked gate value and its position on the waveforms for different retracking approaches.

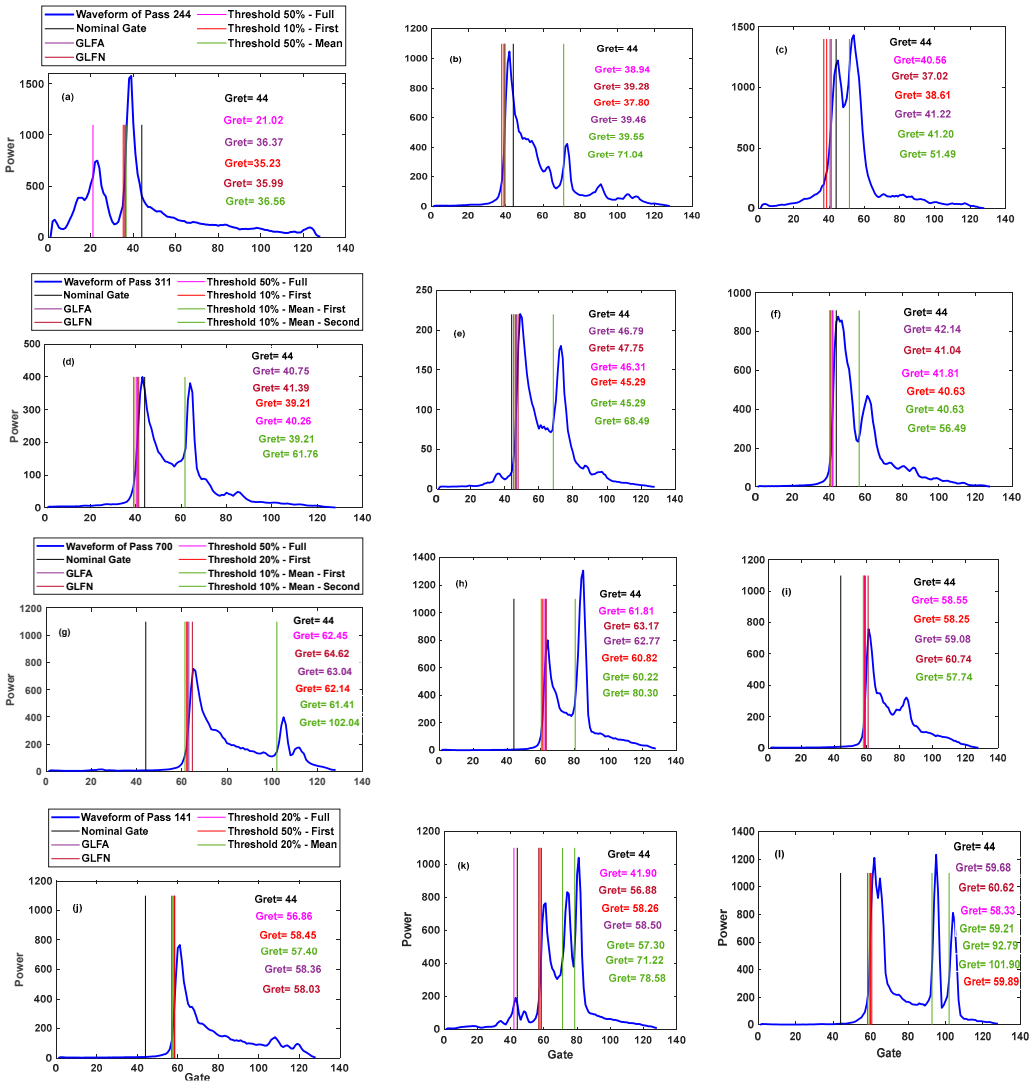

Figure 7. The retracked gate value and its position on the waveform according to the different retracking approaches used in this study; (**a**–**c**) the examples for pass 244 for the Bay of Alcudia; (**d**–**f**) pass 311 for the Northeast Gulf of Bothnia; (**g**–**i**) pass 700 for Hjälmaren Lake; (**j**–**l**) pass 141 for Vättern Lake.

2.6. Water Level Estimation

To generate water level time series for the study areas, the following processes were carried out using the on-board retrackers in the Level-2 Sentinel-3A mission data, full-waveform, first and mean sub-waveform retracking using the threshold retracker, as well as the GLFA and GLFN approaches.

(1) Generating the Instantaneous Water Level Time Series

The instantaneous water level time series for each pass in each cycle were formed using the retracking correction calculated from the threshold retracking algorithm for the full-waveform, the first, the mean sub-waveform, the GLFA/GLFN approaches, as well as for the existing retrackers in Level-2 data. The corrections are applied according to Equation (3).

(2) Identification and Removal of Outliers in the Instantaneous Water Level Time Series

Outliers in the instantaneous water level time series for each pass in each cycle were identified and removed at a 95% confidence level (Figure 8).

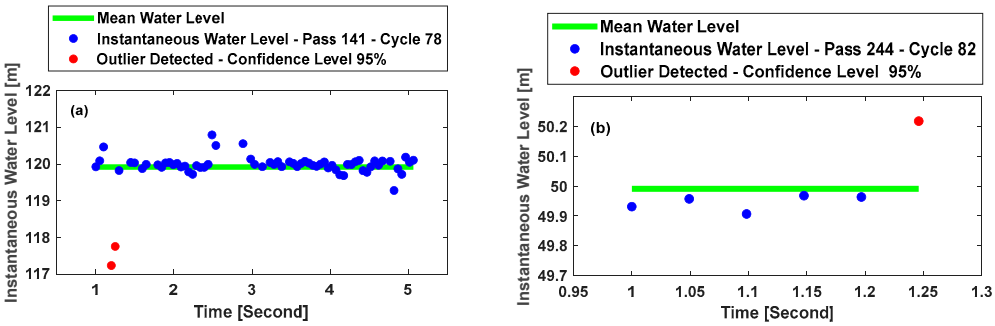

Figure 8. Identification and removal of outliers in the instantaneous water level at a 95% confidence level; (**a**) Cycle 78 of pass 141 in Vättern Lake; (**b**) Cycle 82 of pass 244 in the Bay of Alcudia.

(3) Generation of the Final Time Series of the Water Level for each Pass

After identifying and removing outliers in the previous step, the mean value of the instantaneous water level time series for each satellite overpass was chosen as the representative. By merging the mean value of the water level for different satellite overpasses, the final time series of the water level for each pass was obtained.

(4) Evaluation of the Final Time Series of the Water Level

In the previous step, the final time series of the water level for each pass was obtained from different retracking approaches and from on-board retrackers that exist in the Level-2 data of the Sentinel-3A mission. The water level time series obtained from our retracking scenarios were validated against tide gauge data in terms of RMSE. Additionally, the improvement percentage (IMP%) of RMSE was computed to compare the results of the GLFA and GLFN approaches against the optimum on-board retracker (with minimum RMSE) in the Level-2 data for each study area (Equation (13)). It is worth mentioning that prior to computing RMSE, the bias between the tide gauge and satellite altimetry data was adjusted due to the datum difference.

$$IMP(\%) = \frac{RMSE_{On-borad} - RMSE_{new-approach}}{RMSE_{On-borad}} \times 100 \quad (13)$$

In Equation (12), $RMSE_{new-approach}$ and $RMSE_{On-borad}$ are the RMSEs obtained from comparing the time series of the GLFA and GLFN approaches and the optimum on-board retracker against tide gauge data, respectively.

3. Results and Discussion

3.1. Multi-Peak and Optimal Peak Analysis

The numerical results of the percentage analysis for multi-peak waveforms and optimal peaks for each of the study areas are presented in Table 4, and its circular graph is depicted in Figure 9.

Table 4. The statistical information includes the number (N) and the percentage (%) of multi-peak waveforms, as well as the percentage of the optimal peak number in the study areas.

Case Study	Pass	Single Peak (N)	Multi Peak (N)	Multi Peak (%)	First (%)	Second (%)	Third (%)	Fourth (%)
Bay of Alcudia	244	220	96	30.38	18.04	10.44	1.58	0.32
Northeast Gulf of Bothnia	311	240	75	23.81	19.68	3.81	0.32	0
Hjälmaren Lake	700	1816	619	25.42	22.75	2.59	0.08	0
Vättern Lake	141	2809	1352	32.49	30.35	2.14	0	0

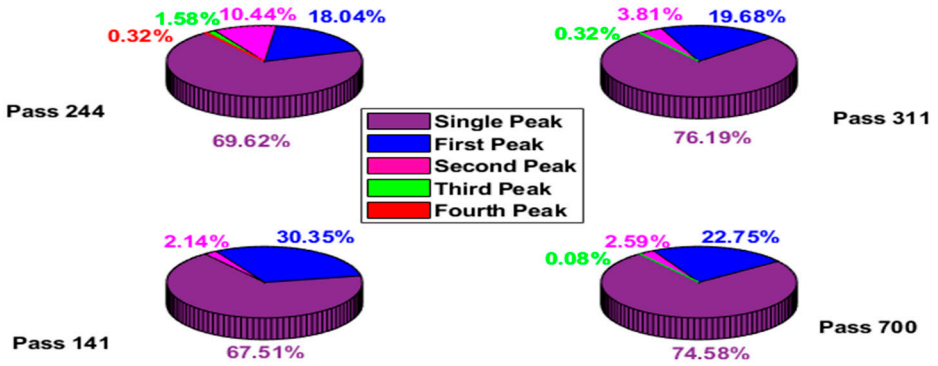

Figure 9. The circular graph shows the percentage analysis of multi-peak waveforms and the optimal peak.

The results in Table 4 indicate that Vättern Lake, the Bay of Alcudia, Hjälmaren Lake, and the Northeast Gulf of Bothnia have the highest, 32.49%, and the lowest, 23.81%, percentages of multi-peak waveforms, respectively. In each of the four study areas, the first peak is predominantly the optimal peak. Vättern Lake, Hjälmaren Lake, the Northeast Gulf of Bothnia, and the Bay of Alcudia are assigned the first optimal peak, from the highest at 30.35% to the lowest at 18.04%, respectively. In Vättern Lake, the optimal peak extends to the second peak; in Hjälmaren Lake and the Northeast Gulf of Bothnia, it spreads to the third peak; and in the Bay of Alcudia, it broadens to the fourth peak. These results demonstrate that the first peak can be the optimal peak but not always; this confirms the results from previous studies [3,6,21–23].

3.2. Evaluation of the Optimal Fitting Parameters

Table 5 represents the results of evaluating the Mean Absolute Error (MAE), Root Mean Square Error (RMSE), and Correlation coefficient (Corr) parameters in the optimal fitting of the GLFN approach to the first sub-waveform. This evaluation was based on comparing the RMSE of the final water level time series obtained from each parameter against the tide gauge data.

Table 5. The RMSE values (cm) between the final water level time series and tide gauge data obtained using the evaluation parameters MAE, RMSE, and Corr in the GLFN approach.

Case Study (Pass)-Parameter	MAE	RMSE	Corr
Bay of Alcudia (244)	31	31	**31**
Northeast Gulf of Bothnia (311)	81	77	**56**
Hjälmaren Lake (700)	61	65	**10**
Vättern Lake (141)	11	12	**8**

The results in Table 5 indicate the superiority of the Corr evaluation parameter compared to the other parameters, with values of 8 cm in Vättern Lake, 10 cm in Hjälmaren Lake, and 56 cm in the Northeast Gulf of Bothnia. Additionally, for the Bay of Alcudia, an equivalent result of 31 cm was obtained for all three parameters. Therefore, the Corr evaluation parameter became the criterion for the GLFN approach.

3.3. Evaluation of the Water Level Time Series Obtained from Our Retracking Approaches

Tables 6–9 present the RMSE (m) values of the final water level time series for passes 244, 141, 311, and 700 of the Sentinel-3A missions, respectively, for the Bay of Alcudia, the Northeast Gulf of Bothnia, Vättern, and Hjälmaren Lakes compared to the tide gauge data. These RMSEs values represent all the retracking scenarios discussed in this study.

The results in Table 6 indicate that in the study areas of the Bay of Alcudia, the Ocean physical retracker performed better with an RMSE of 0.58 m compared to other on-board retrackers. This retracker performs almost the same as the empirical OCOG retracker, with an RMSE of 0.59 m. The threshold retracker in the approaches of full-waveform, first sub-waveform, and mean sub-waveform, respectively, achieved the lowest RMSE values of 0.95 m for a threshold of 50%, 0.99 m for a threshold of 10%, and 0.73 m for a threshold of 50%. The GLFA approach had better performance with an RMSE of 0.11m compared to the GLFN approach with an RMSE of 0.31m.

Table 6. The RMSE (m) values for the final water level time series of the Bay of Alcudia obtained from the retracking approaches (Full-waveform and First and Mean sub-waveform retracking) in this study.

Retracker Approach	Full	First	Mean
Ocean	0.58	-	-
Tracker	0.77	-	-
OCOG	0.59	-	-
Sea-ice	0.62	-	-
Ice-sheet	0.62	-	-
Threshold 10%	1.37	0.99	0.74
Threshold 20%	1.41	1	0.74
Threshold 50%	0.95	1	0.73
GLFA	-	**0.11**	-
GLFN	-	0.31	-

As it is clear from the final water level time series results for the Northeast Gulf of Bothnia in Table 7, the Ice-sheet mathematical retracker achieved the optimal outcome with an RMSE of 0.56 m compared to other on-board retrackers available in the Level-2 data. The threshold retracking algorithm in the full-waveform approach with a 50% threshold provided the lowest RMSE of 0.71 m. This algorithm with the first and mean sub-waveform approaches yielded RMSE values of 1.18 and 1.42 with different thresholds and a 10% threshold, given in order. GLFA and GLFN also provided RMSE values of 0.36 m and 0.56 m, sequentially.

Table 7. The RMSE (m) values for the final water level time series of the Northeast Gulf of Bothnia obtained from the retracking approaches (Full-waveform and First and Mean sub-waveform retracking) in this study.

Retracker Approach	Full	First	Mean
Ocean	1.43	-	-
Tracker	1.58	-	-
OCOG	0.6	-	-
Sea-ice	3.20	-	-
Ice-sheet	0.56	-	-
Threshold 10%	3.27	1.18	1.42
Threshold 20%	2.94	1.18	1.45
Threshold 50%	0.71	1.18	1.47
GLFA	-	**0.36**	-
GLFN	-	0.56	-

From the results in Table 8 for Hjälmaren Lake, it can be inferred that the empirical OCOG retracker with an RMSE of 0.15 m and the threshold retracker in the full-waveform and first sub-waveform approaches with thresholds of 50% and 20%, respectively, yielded nearly equivalent results with RMSE values of 0.14 m. The threshold retracking algorithm with a 10% threshold in the mean sub-waveform approach resulted in an RMSE of 0.89 m.

GLFA and GLFN also demonstrated similar performances, with RMSE values of 0.09 m and 10 m, in the prescribed order.

Table 8. The RMSE (m) values for the final water level time series of Hjälmaren Lake obtained from the retracking approaches (Full-waveform and First and Mean sub-waveform retracking) in this study.

Retracker Approach	Full	First	Mean
Ocean	0.41	-	-
Tracker	1.86	-	-
OCOG	0.15	-	-
Sea-ice	0.30	-	-
Ice-sheet	0.23	-	-
Threshold 10%	0.84	0.16	0.89
Threshold 20%	0.56	0.14	0.91
Threshold 50%	0.14	0.15	0.94
GLFA	-	**0.09**	-
GLFN	-	0.10	-

The results in Table 9 regarding the processing of Vättern Lake data indicate that the Sea-ice mathematical on-board retracker, with a 20% threshold in the full-waveform retracking approach, a 50% threshold in the first sub-waveform retracking approach, and thresholds of 20% and 50% in the mean sub-waveform retracking approach, yielded the best RMSE values of 0.19 m, 0.28 m, 0.09 m, and 1.19 m, respectively. The GLFA and GLFN approaches also exhibited almost equivalent performances, with RMSE values of 0.09 m and 0.08 m, given in order.

Table 9. The RMSE (m) values for the final water level time series of Vättern Lake obtained from the retracking approaches (Full-waveform and First and Mean sub-waveform retracking) in this study.

Retracker Approach	Full	First	Mean
Ocean	1.07	-	-
Tracker	1.53	-	-
OCOG	0.61	-	-
Sea-ice	0.19	-	-
Ice-sheet	0.66	-	-
Threshold 10%	0.62	0.1	1.20
Threshold 20%	0.28	0.1	1.19
Threshold 50%	0.35	0.09	1.19
GLFA	-	0.09	-
GLFN	-	**0.08**	-

Table 10 provides a summary of the optimal results from Tables 6–9. It presents the best result obtained from different retracking scenarios implemented in our study. Additionally, it includes the improvement percentage in RMSE between the results obtained from the two GLFA and GLFN approaches compared to the optimal outcome of on-board retrackers.

The results in Table 10 indicate that in the Bay of Alcudia and the Northeast Gulf of Bothnia, the on-board retracker performs better with RMSE values of 0.58 m and 0.56 m, respectively, compared to the full-waveform retracking, first sub-waveform retracking, and mean sub-waveform retracking approaches. In Vättern Lake, on-board retrackers outperform the full-waveform and mean sub-waveform retracking approaches. For Hjälmaren Lake, the on-board retracker almost has the same performance as the full-waveform and first sub-waveform retracking approaches. The appropriate results of the on-board retracker indicate that the waveforms in these study areas have a high level of agreement with the assumptions of the on-board retrackers, which are explained in Section 2.4.

Table 10. The optimal RMSE (m) results for the different retracking approaches used in this study.

Approach-Case Study (Pass)	Bay of Alcudia (244)	Northeast Gulf of Bothnia (311)	Vättern Lake (141)	Hjälmaren Lake (700)
On-board retracker	0.58	0.56	0.19	0.15
Full	0.95	0.71	0.28	0.14
First	0.99	1.18	0.09	0.14
Mean	0.73	1.42	1.19	0.89
GLFA/IMP%	**0.11/81**	**0.36/36**	0.09/53	**0.09/40**
GLFN/IMP%	0.31/46	0.56/0	**0.08/58**	0.10/33

The difference between the RMSE results of the first and mean sub-waveform retracking approaches is less for the Northeast Gulf of Bothnia and the Bay of Alcudia than for Hjälmaren Lake and Vättern Lake. This arrangement applies to the amount of optimal sub-waveform expended, as mentioned in Table 4. In other words, the optimal peak is more expanded (the optimal peak number has increased), and the mean sub-waveform retracking approach has almost obtained closer results to the first sub-waveform retracking approach. The retracking of the mean sub-waveform performed better only in the Bay of Alcudia (the maximum extended optimal sub-waveform) compared to the retracking of the first sub-waveform, while in the other three areas, the superior performance of retracking the first sub-waveform is evident. In Vättern Lake (the minimum extended optimal sub-waveform), the difference between the RMSE result of the first and mean sub-waveform retracking approaches is the largest.

In Vättern Lake, with the lowest extended optimal peak, the GLFN provided an almost similar performance with an RMSE of 0.08 m compared to the GLFA and the retracking of the first sub-waveform using the threshold retracker with an RMSE of 0.09 m. In the three other study areas, namely the Bay of Alcudia, the Northeast Gulf of Bothnia, and Hjälmaren Lake, the optimal peak stretches to the third and fourth peaks. In this case, it is more likely that the first sub-waveform is ambiguous. Therefore, in the dissimilarity step, the ambiguous waveforms were excluded, and accordingly, the GLF performed better compared to other retracking approaches discussed in this study, especially the first sub-waveform retracking approach that was the optimal approach in the previous study. This issue also confirms that the first peak will not always be the optimal peak and confirms the results of previous studies [3,6,21–23]. It is important to note that the performance of the threshold retracker depends on the selected threshold value, which is determined empirically. The optimal threshold may vary for different study areas. Therefore, selecting the threshold value in this method is a challenge. Nevertheless, the GLF retracker is independent of empirical values.

In coastal areas, the GLFA approach performed better than the GLFN approach, and over the lakes, the results were nearly equivalent for these two approaches. This result demonstrates the relative superiority of the GLFA approach over the GLFN approach. The performance of the GLFN approach is dependent on the computed slope value for the ascending section, the assessment steps of the retracking gate, and the evaluation parameter to determine the optimal retracking gate. In contrast, the GLFA approach is independent of these limitations.

In its optimized approach (analytical or numerical), the GLF approach led to improvements of 81%, 36%, 58%, and 40% in the accuracy of the water level time series compared to the on-board retrackers. Therefore, in all study areas, GLF outperformed the retrackers available in the Level-2 data.

Figure 10 illustrates the final optimal water level time series for the various investigated approaches and study areas in this study.

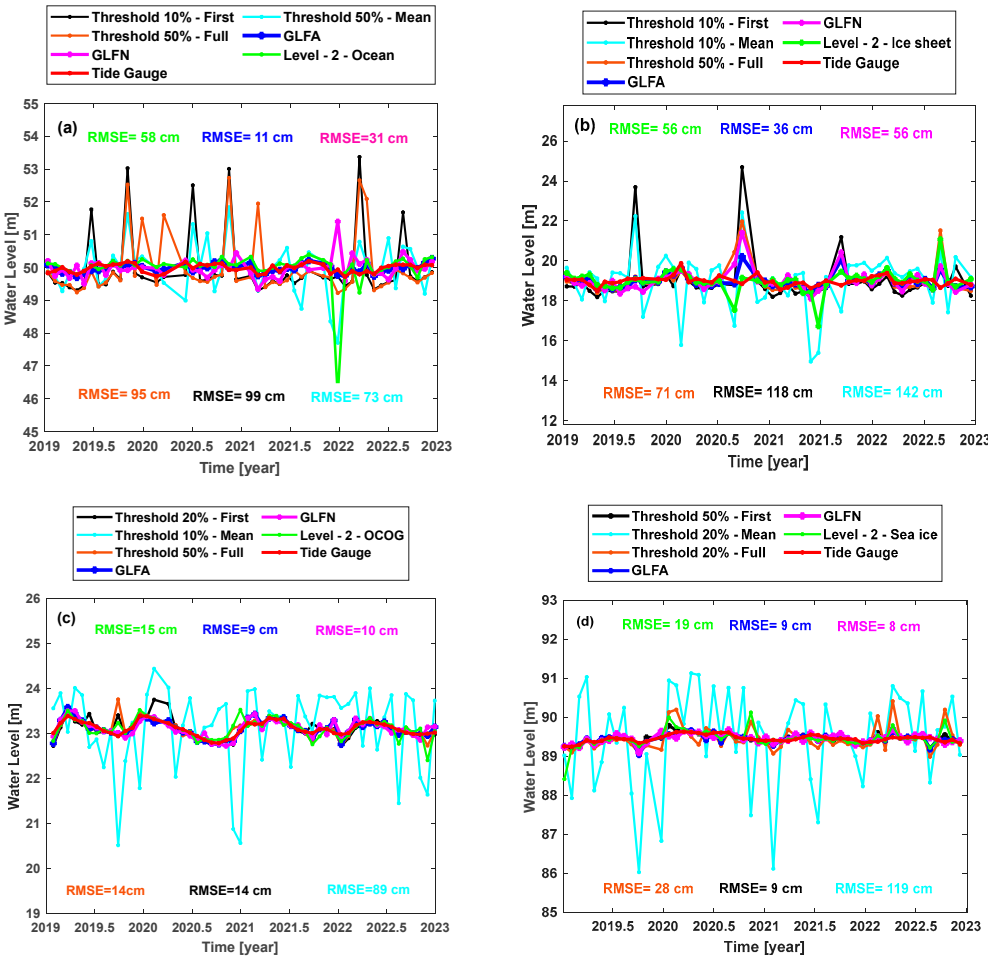

Figure 10. Final optimal water level time series for the various investigated approaches and study areas in this research; (**a**) the Bay of Alcudia, (**b**) the Northeast Gulf of Bothnia, (**c**) Hjälmaren Lake, and (**d**) Vättern Lake.

4. Conclusions

The waveforms of satellite altimetry in inland water bodies and coastal areas often deviate from the ideal oceanic waveform due to factors such as shallow water depths and the presence of non-aqueous features within the satellite footprint. To retrieve accurate water level time series in these regions, retracking methods are essential. Previous studies have highlighted the potential of using new generation satellite altimetry missions, such as Sentinel-3 operating in SAR mode, combined with the threshold retracker applied to the first sub-waveform [3,6,9,19–21,37,38]. The threshold value in this retracker is typically set at 10%, 20%, or 50% [12], though alternative values have been explored [3,9,16,19,50]. However, selecting the optimal threshold value and the appropriate sub-waveform remains a challenge, as some studies have suggested that the first sub-waveform may not always be the best option [3,21,23]. In this study, where ambiguity in selecting the first sub-waveform was identified, waveforms were excluded from processing using a Generalized Logistic Function (GLF) and a dissimilarity parameter. The remaining waveforms were retracked using the GLFA and GLFN methods. The results of these proposed methods were compared against existing retracking algorithms in the Level-2 data, as well as the threshold retracking of the full-waveform, first sub-waveform, and mean sub-waveform. These approaches were evaluated against tide gauge data using Sentinel-3A mission passes (244, 311, 700, and 141) over the Bay of Alcudia, the Northeast Gulf of Bothnia (0–2 km from the coast), and the Lakes of Hjälmaren and Vättern in Sweden. The findings demonstrate the potential

of the proposed methodology to improve water level retrievals in complex inland and coastal regions.

- Retracking the waveforms of satellite altimetry to generate accurate water level time series is essential for inland water bodies and coastal areas;
- The first sub-waveform in the waveforms is often optimal for retracking but not always. Therefore, the first sub-waveform of waveforms must be retracked where the choice of the first sub-waveform is unambiguous;
- Retracking the first unambiguous sub-waveform using the GLF approach in the optimal scenario (GLFA or GLFN) has improved the RMSE compared to on-board retrackers for all study areas by 81%, 36%, 58%, and 40% for the Bay of Alcudia, the Northeast Gulf of Bothnia, Vättern Lake, and Hjälmaren Lake, sequentially;
- In the coastal areas studied in this research, GLFA performed better than GLFN, and their performance was nearly equivalent in lakes. The performance of the GLFN approach, unlike the GLFA, depends on the determination of the slope for the ascending section, the step size for retracking gate assessment, and the evaluation parameter for finding the optimal retracking gate;
- In all study areas, retracking the first unambiguous sub-waveform using the GLF approach has shown better results compared to on-board retrackers, such as the full-waveform approach and the first and mean sub-waveform retracking approaches using the threshold algorithm, except for Vättern Lake, where the results were almost equivalent to the first sub-waveform retracking approach.
- The results of the threshold algorithm depend on the selection of the empirical threshold value. GLF does not require entering an empirical value in any of the approaches;
- The investigation of various retracking approaches in this research often shows the poor performance of the mean sub-waveform retracking approach compared to other retracking methods.

Author Contributions: Conceptualization, A.A., D.D.M., and B.V.; formal analysis, S.R., A.A., B.V., M.A.K., and M.P.; writing—original draft, A.A., B.V., M.A.K., and M.P.; supervision—review and editing, D.D.M., B.V, and S.R; All authors have read and agreed to the published version of the manuscript.

Funding: This research received no external funding.

Data Availability Statement: The datasets generated and analyzed during the current study are available from the corresponding author upon reasonable request.

Conflicts of Interest: Author Shirzad Roohi was employed by the company Innovation Solutions-GMV. The remaining authors declare that the research was conducted in the absence of any commercial or financial relationships that could be construed as a potential conflict of interest.

References

1. Zheng, J.; Xu, X.-Y.; Xu, Y.; Guo, C. Coastal Waveform Retracking for Synthetic Aperture Altimeters Using a Multiple Optimization Parabolic Cylinder Algorithm. *Remote Sens.* **2023**, *15*, 4665. [CrossRef]
2. Fabris, M.; Balin, M.; Monego, M. High-Resolution Real-Time Coastline Detection Using GNSS RTK, Optical, and Thermal SfM Photogrammetric Data in the Po River Delta, Italy. *Remote Sens.* **2023**, *15*, 5354. [CrossRef]
3. Roohi, S.; Amini, A.; Voosoghi, B.; Battles, D. Lake Monitoring from a Combination of Multi Copernicus Missions: Sentinel-1 A and B and Sentinel-3A. *J. Hydrogeol. Hydrog. Energy* **2019**, *8*, 3.
4. Vignudelli, S.; Scozzari, A.; Abileah, R.; Gómez-Enri, J.; Benveniste, J.; Cipollini, P. Water surface elevation in coastal and inland waters using satellite radar altimetry. In *Extreme Hydroclimatic Events and Multivariate Hazards in a Changing Environment*; Elsevier: Amsterdam, The Netherlands, 2019; pp. 87–127.
5. Shiklomanov, A.; Lammers, R.; Vörösmarty, C.J. Widespread decline in hydrological monitoring threatens pan-Arctic research. *Eos Trans. Am. Geophys. Union* **2002**, *83*, 13–17. [CrossRef]

6. Roohi, S. Capability of Pulse-Limited Satellite Radar Altimetry to Monitor Inland Water Bodies. Master's Thesis, University of Stuttgart, Stuttgart, Germany, 2015.
7. Calmant, S.; Crétaux, J.-F.; Rémy, F. Principles of Radar Satellite Altimetry for Application on Inland Waters. In *Microwave Remote Sensing of Land Surface*; Elsevier: Amsterdam, The Netherlands, 2017; pp. 175–218.
8. Brown, G. The average impulse response of a rough surface and its applications. *IEEE Trans. Antennas Propag.* **1977**, *25*, 67–74. [CrossRef]
9. Agar, P.; Roohi, S.; Voosoghi, B.; Amini, A.; Poreh, D. Sea Surface Height Estimation from Improved Modified, and Decontaminated Sub-Waveform Retracking Methods over Coastal Areas. *Remote Sens.* **2023**, *15*, 804. [CrossRef]
10. Martin, T.V.; Zwally, H.J.; Brenner, A.C.; Bindschadler, R.A. Analysis and retracking of continental ice sheet radar altimeter waveforms. *J. Geophys. Res. Ocean.* **1983**, *88*, 1608–1616. [CrossRef]
11. Wingham, D.; Rapley, C.; Griffiths, H. New techniques in satellite altimeter tracking systems. In Proceedings of the IGARSS, Zürich, Switzerland, 8–11 September 1986; pp. 1339–1344.
12. Davis, C.H. A robust threshold retracking algorithm for measuring ice-sheet surface elevation change from satellite radar altimeters. *IEEE Trans. Geosci. Remote Sens.* **1997**, *35*, 974–979. [CrossRef]
13. Hwang, C.; Guo, J.; Deng, X.; Hsu, H.-Y.; Liu, Y. Coastal gravity anomalies from retracked Geosat/GM altimetry: Improvement, limitation and the role of airborne gravity data. *J. Geod.* **2006**, *80*, 204–216. [CrossRef]
14. Jinyum, G.; Cheiway, H.; Xiaotao, C.; Yuting, L. Improved threshold retracker for satellite altimeter waveform retracking over coastal sea. *Prog. Nat. Sci.* **2006**, *16*, 732–738. [CrossRef]
15. Guo, J.; Chang, X.; Gao, Y.; Sun, J.; Hwang, C. Lake level variations monitored with satellite altimetry waveform retracking. *IEEE J. Sel. Top. Appl. Earth Obs. Remote Sens.* **2009**, *2*, 80–86. [CrossRef]
16. Yang, Y.; Hwang, C.; Hsu, H.-J.; Dongchen, E.; Wang, H. A subwaveform threshold retracker for ERS-1 altimetry: A case study in the Antarctic Ocean. *Comput. Geosci.* **2012**, *41*, 88–98. [CrossRef]
17. Jain, M.; Andersen, O.B.; Dall, J.; Stenseng, L. Sea surface height determination in the Arctic using Cryosat-2 SAR data from primary peak empirical retrackers. *Adv. Space Res.* **2015**, *55*, 40–50. [CrossRef]
18. Ganguly, D.; Chander, S.; Desai, S.; Chauhan, P. A subwaveform-based retracker for multipeak waveforms: A case study over Ukai dam/reservoir. *Mar. Geod.* **2015**, *38*, 581–596. [CrossRef]
19. Villadsen, H.; Deng, X.; Andersen, O.B.; Stenseng, L.; Nielsen, K.; Knudsen, P. Improved inland water levels from SAR altimetry using novel empirical and physical retrackers. *J. Hydrol.* **2016**, *537*, 234–247. [CrossRef]
20. Yang, Y.; Moore, P.; Li, Z.; Li, F. Lake Level Change From Satellite Altimetry Over Seasonally Ice-Covered Lakes in the Mackenzie River Basin. *IEEE Trans. Geosci. Remote Sens.* **2020**, *59*, 8143–8152. [CrossRef]
21. Roohi, S. Performance Evaluation of Different Satellite Radar Altimetry Missions for Monitoring Inland Water Bodies. Ph.D. Thesis, University of Stuttgart, Stuttgart, Germany, 2017.
22. Roohi, S.; Sneeuw, N.; Benveniste, J.; Dinardo, S.; Issawy, E.; Zhang, G. Evaluation of CryoSat-2 water level derived from different retracking scenarios over selected inland water bodies. *Adv. Space Res.* **2019**, *68*, 947–962. [CrossRef]
23. Mafi, S.; Farzaneh, S.; Sharifi, M.A.; Forootan, E. Spline retracker: A geometrical retracking algorithm for coastal and open ocean altimetry. *Mar. Geod.* **2023**, *47*, 83–118. [CrossRef]
24. Passaro, M.; Cipollini, P.; Vignudelli, S.; Quartly, G.D.; Snaith, H.M. ALES: A multi-mission adaptive subwaveform retracker for coastal and open ocean altimetry. *Remote Sens. Environ.* **2014**, *145*, 173–189. [CrossRef]
25. Verhulst, P.-F. Notice sur la loi que la population suit dans son accroissement. *Corresp. Math. Phys.* **1838**, *10*, 113–129.
26. Verhulst, P.-F. Recherches mathématiques sur la loi d'accroissement de la population. *Mémoires L'académie R. Belg.* **1845**, *18*, 1–40. [CrossRef]
27. Cramer, J.S. The Origins of Logistic Regression. 2002. Available online: https://papers.tinbergen.nl/02119.pdf (accessed on 28 September 2024).
28. Bacaër, N. Verhulst and the logistic equation (1838). In *A Short History of Mathematical Population Dynamics*; Springer: London, UK, 2011; pp. 35–39.
29. Ramos, R.A. Logistic function as a forecasting model: It's application to business and economics. *Int. J. Eng.* **2013**, *2*, 2305–8269.
30. Yamak, Y.; Kılıçaslan, M.; Demirci, R. Image filter with logistic functions. In Proceedings of the 2020 4th International Symposium on Multidisciplinary Studies and Innovative Technologies (ISMSIT), Istanbul, Turkey, 22–24 October 2020; pp. 1–5.
31. Villanueva, D.; Feijóo, A. Comparison of logistic functions for modeling wind turbine power curves. *Electr. Power Syst. Res.* **2018**, *155*, 281–288. [CrossRef]
32. Kudryashov, N.A. Logistic function as solution of many nonlinear differential equations. *Appl. Math. Model.* **2015**, *39*, 5733–5742. [CrossRef]
33. Xu, Y. Using logistic function to predict epidemic trend of COVID-19 in China. In Proceedings of the International Conference on Mathematical Physics and Computational Simulation, Oxford, UK, 12–18 August 2023.
34. Rządkowski, G.; Sobczak, L. A generalized logistic function and its applications. *Found. Manag.* **2020**, *12*, 85–92. [CrossRef]

35. EUMETSAT. *Sentinel-3 SRAL Marine User Handbook*; EUMETSAT: Darmstadt, Germany, 2017; p. 55.
36. Raney, R.K. The delay/Doppler radar altimeter. *IEEE Trans. Geosci. Remote Sens.* **1998**, *36*, 1578–1588. [CrossRef]
37. Jensen, J.; Raney, R. Multi-mission radar altimeter: Concept and performance. In Proceedings of the Geoscience and Remote Sensing Symposium, 1996, IGARSS'96, Remote Sensing for a Sustainable Future, Lincoln, NE, USA, 31 May 1996; pp. 2279–2281.
38. Martin-Puig, C.; Marquez, J.; Ruffini, G.; Raney, R.K.; Benveniste, J. SAR altimetry applications over water. *arXiv* **2008**, arXiv:0802.0804.
39. Dinardo, S.; Fenoglio-Marc, L.; Buchhaupt, C.; Becker, M.; Scharroo, R.; Fernandes, M.J.; Benveniste, J. Coastal sar and plrm altimetry in german bight and west baltic sea. *Adv. Space Res.* **2018**, *62*, 1371–1404. [CrossRef]
40. Team, S. *Sentinel-3 User Handbook*; European Space Agency: Paris, France, 2013; Volume 150.
41. LAKEPEDIA. Available online: https://www.lakepedia.com/ (accessed on 19 April 2024).
42. Available online: https://wldb.ilec.or.jp/ (accessed on 19 April 2024).
43. Mallorca Facts. Available online: https://mallorca.com/en/travel-info/shopping/mallorca-facts-figures (accessed on 20 April 2024).
44. Gulf of Bothnia. Available online: https://www.britannica.com/place/Gavleborg (accessed on 21 April 2024).
45. Yuan, C.; Gong, P.; Zhang, H.; Guo, H.; Pan, B. Monitoring water level changes from retracked Jason-2 altimetry data: A case study in the Yangtze River, China. *Remote Sens. Lett.* **2017**, *8*, 399–408. [CrossRef]
46. Arabsahebi, R.; Voosoghi, B.; Tourian, M.J. The inflection-point retracking algorithm: Improved Jason-2 sea surface heights in the Strait of Hormuz. *Mar. Geod.* **2018**, *41*, 331–352. [CrossRef]
47. Khaki, M.; Forootan, E.; Sharifi, M.A. Satellite radar altimetry waveform retracking over the Caspian Sea. *Int. J. Remote Sens.* **2014**, *35*, 6329–6356. [CrossRef]
48. Tourian, M.J. Controls on Satellite Altimetry Over Inland Water Surfaces for Hydrological Purposes. Master's Thesis, University of Stuttgart, Stuttgart, Germany, 2012.
49. Mikhail, E.M.; Ackermann, F.E. *Observations and Least Squares*; International Engineering Publications, University Press of America: Lanham, MD, USA, 1976.
50. Khajeh, S.; Jazireeyan, I.; Ardalan, A.A. Applying satellite altimetry to wetland water levels monitoring (case study: Louisiana wetland). *IEEE Geosci. Remote Sens. Lett.* **2014**, *11*, 1475–1478. [CrossRef]